Ultrasonics 138 (2024) 107229

Contents lists available at ScienceDirect

Ultrasonics

journal homepage: www.elsevier.com/locate/ultras

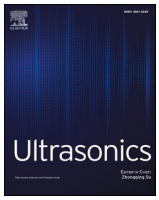

"Cumulative effect" of second harmonic Lamb waves in a lossy plate

Shengbo Shan [a,*], Yuanman Zhang [b], Liaoliao Cheng [a], Yang Song [b], Yongdong Pan [a], Li Cheng [b,c,*]

[a] School of Aerospace Engineering and Applied Mechanics, Tongji University, Shanghai 200092, People's Republic of China
[b] Department of Mechanical Engineering, The Hong Kong Polytechnic University, Kowloon, Hong Kong
[c] Hong Kong Branch of National Rail Transit Electrification and Automation Engineering Technology Research Center, The Hong Kong Polytechnic University, Kowloon, Hong Kong

ARTICLE INFO

Keywords:
Lamb waves
Second harmonic
Cumulative effect
Wave attenuation
Material damping

ABSTRACT

The second harmonic Lamb waves have high sensitivity to microstructural defects in materials and are therefore promising for incipient damage detection and monitoring of thin-walled structures. Existing studies have shown that the second harmonic Lamb waves can be cumulative with increasing propagation distance under the internal resonance conditions, which is conducive to nonlinear wave measurements in view of structural health monitoring. However, when propagating in a lossy structure with damping, the cumulative properties of the second harmonic Lamb waves are affected by energy dissipation and thus need to be re-examined. In this paper, a method for predicting the cumulative characteristics of second harmonic Lamb waves in damped plates is proposed. Instead of using material damping parameters which are difficult to obtain in practice, the proposed method relies on the attenuation patterns of Lamb waves at fundamental and double frequencies while taking into account the influence of the wave beam divergence. The proposed methodology is validated by finite element simulations and experiments. The results show that the cumulative second harmonic Lamb waves in the damped plate tend to increase and then decrease, and a "sweet" zone of relatively large amplitude can be predicted using the proposed method. The elucidation of the cumulative characteristics of the second harmonic Lamb waves provides guidance for effective system design for structural damage detection and monitoring applications.

1. Introduction

Material nonlinearity, which is characterized by the macroscale nonlinear stress–strain relationship, usually arises from microstructural defects such as lattice anomalies, dislocations, microcracks, *etc.* [1–3]. With guided waves propagating in thin-walled structures like a plate with material nonlinearity, nonlinear components are generated such as higher harmonics and mixed-frequency components [4–7]. Due to their generation mechanism, nonlinear guided waves are inherently sensitive to changes in material microstructure and therefore hold great promise for non-destructive evaluation (NDE) and structural health monitoring (SHM) applications [8–11].

Among various types of nonlinear guided waves, the second harmonic Lamb waves have been widely studied and exploited for NDE and SHM applications [8,12]. For example, Li et al. proposed a damage localization algorithm to identify and image a micro-defect in a 1060 aluminum plate according to the phase matching conditions of the S0 mode second harmonic Lamb waves [13]. Chen et al. also used the S0 mode second harmonic Lamb waves to characterize the interfacial property of a double-layer plate (two metal plates bonded with epoxy) subjected to different annealing conditions [14]. Masurkar et al. used the internally resonant second harmonic Lamb waves (S1-S2 mode pair) to monitor the material microstructural changes in Al 7075-T651 plate during fatigue [15].

As a prerequisite to NDE and SHM applications, it is crucial to understand the propagation characteristics of the second harmonic Lamb waves. Existing work has shown that the second harmonic Lamb waves generated by distributed material nonlinearity can be cumulative with the propagation distance if the internal resonance conditions are satisfied [16–19]. Specifically, this requires non-zero power flux from fundamental to second harmonic waves and the phase velocity matching between them. The cumulative effect is of great benefit to NDE and SHM applications for two reasons: 1) the energy of the second harmonic Lamb waves accumulates with propagation distance which facilitates their

* Corresponding authors.
E-mail addresses: shanshengbo@tongji.edu.cn (S. Shan), li.cheng@polyu.edu.hk (L. Cheng).

https://doi.org/10.1016/j.ultras.2023.107229
Received 14 September 2023; Received in revised form 27 November 2023; Accepted 15 December 2023
Available online 16 December 2023
0041-624X/

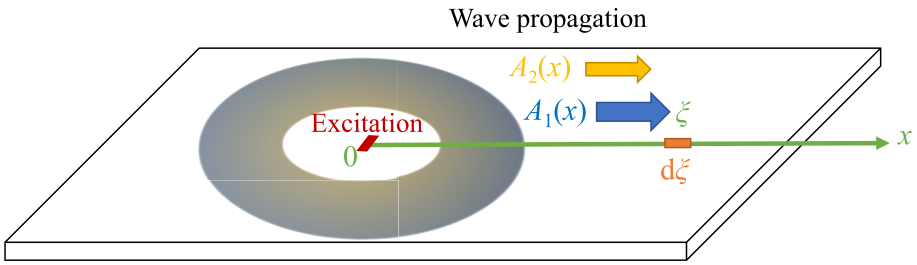

Fig. 1. Sketch of linear and nonlinear Lamb wave propagation in a damped plate.

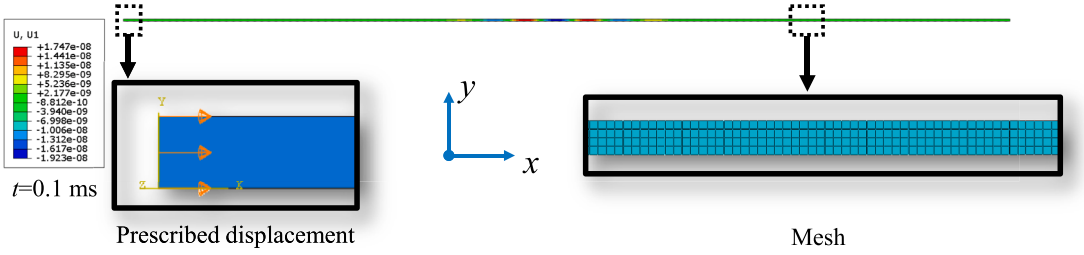

Fig. 2. 2D finite element model.

Table 1
Material parameters for simulations.

ρ[kg/m^3]	λ[GPa]	μ[GPa]	$\tilde{\lambda}$[Pa·s]	$\tilde{\mu}$[Pa·s]	$\bar{A}$[GPa]	$\bar{B}$[GPa]	$\bar{C}$[GPa]
2700	55.27	25.95	2500	1000	–351.2	–149.4	–102.8

measurement; 2) the cumulative feature can be used as an indicator of incipient damage incurred in structures. In practice, only a limited number of fundamental-second harmonic Lamb wave mode pairs strictly satisfy the internal resonance conditions [20]. Apart from these identified mode pairs, the S0 mode Lamb waves have recently been found to approximately meet the internal resonance conditions due to their slightly dispersive nature at low frequencies [21,22]. As a result, the corresponding second harmonic S0 mode Lamb waves are deemed quasi-cumulative with the wave propagation distance. This provides considerable flexibility in the choice of excitation frequencies in practical applications. It is worth noting that the internal resonance conditions for the cumulative effect apply to Lamb waves in both isotropic and anisotropic plates, as demonstrated in [23].

Most of the existing studies focus on the cumulative second harmonic Lamb waves without considering the effect of material damping. When material damping is taken into account, the amplitude of the primary Lamb waves is attenuated during propagation. As a result, the cumulative characteristics of the second harmonic Lamb waves are affected. To address this issue, Kanda and Sugiura proposed a theoretical framework to investigate the amplitude variation of internally-resonant second harmonic waves as a function of the wave propagation distance [24]. Considering the effect of material damping, the amplitude of the second harmonic Lamb waves first increases and then decreases. That work is only a theoretical investigation and still lacks experimental validation. In addition, in practical applications, it is difficult to obtain the accurate

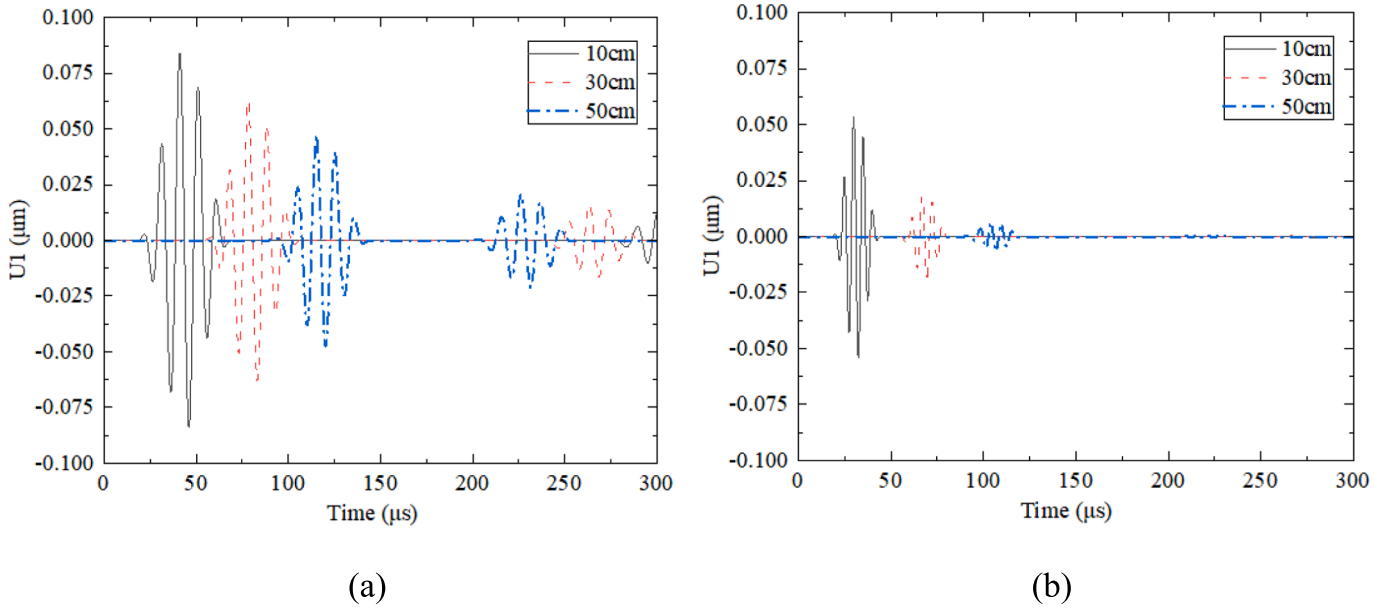

Fig. 3. Typical responses at different locations to the excitations at (a) 100 kHz and (b) 200 kHz.

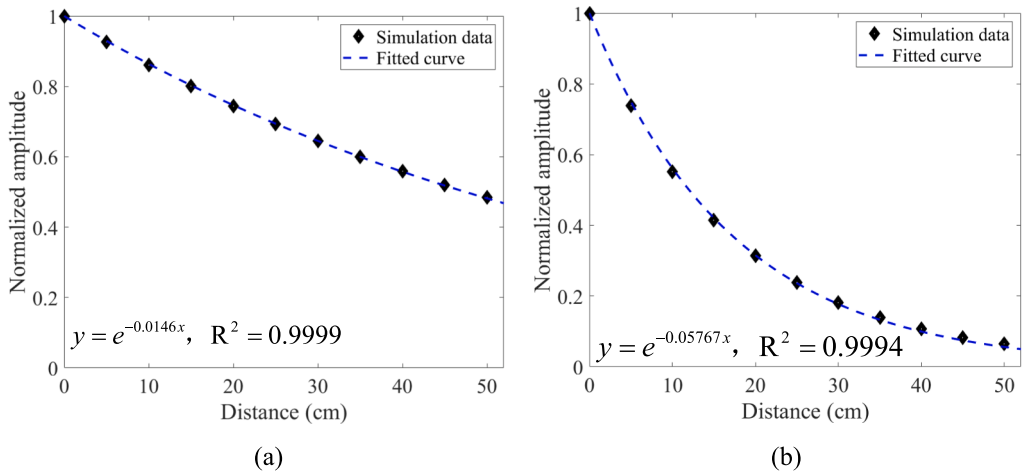

Fig. 4. Characterization of attenuation patterns of Lamb waves at (a) 100 kHz and (b) 200 kHz.

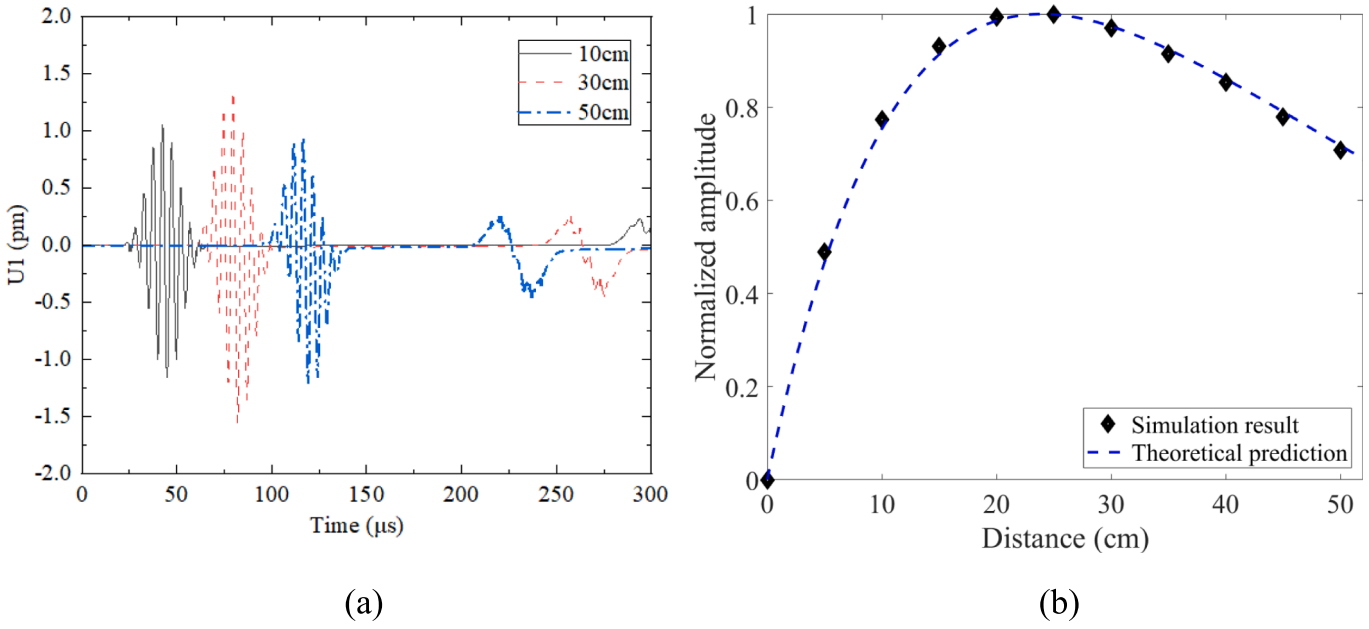

Fig. 5. Cumulative effect of the second harmonic Lamb waves: (a) Typical second harmonic responses (b) comparison between the theoretical prediction and numerical data.

material damping parameters, so the proposed method is difficult to use to guide practical damage monitoring applications.

Motivated by this, we propose a simple method to predict the cumulative feature of the second harmonic Lamb waves, by considering the lossy effect of material damping in a plate. Theoretical analyses are first performed to explain the concept of the proposed method. Numerical simulations are then presented to demonstrate the method with two-dimensional cases. Three-dimensional studies are further considered to investigate the influence of wave beam divergence. Finally, experiments are carried out on a composite plate to further validate the proposed method.

2. Prevailing ideas for predicting cumulative features

Consider the propagation of a plane fundamental Lamb wave in a weakly nonlinear plate. As the wave propagates, the second harmonic Lamb wave is generated, as sketched in Fig. 1. In the absence of damping, without loss of generality, the amplitude of the cumulative second harmonic Lamb wave A_2 can be written as

$$A_2(x) = kA_1^2 x \tag{1}$$

where A_1 and x are the amplitude of the fundamental wave and the propagation distance, respectively. The coefficient k denotes the generation efficiency of the second harmonic Lamb wave, which is related to the elastic constants of materials and wave structures of the fundamental and second harmonic Lamb waves [20].

In a lossy medium where material damping should be considered, both fundamental and second harmonic Lamb waves are attenuated during propagation. Specifically, the attenuation patterns of the linear waves at fundamental and double frequencies are characterized by the functions $f_\omega(\xi)$ and $f_{2\omega}(\xi)$, in which ξ stands for the position. For a segment $d\xi$ at position ξ, the fundamental wave amplitude should be $A_1 f_\omega(\xi)$. Accordingly, the second harmonic Lamb wave amplitude generated by the segment is

$$dA_2 = k(A_1 f_\omega(\xi))^2 d\xi \tag{2}$$

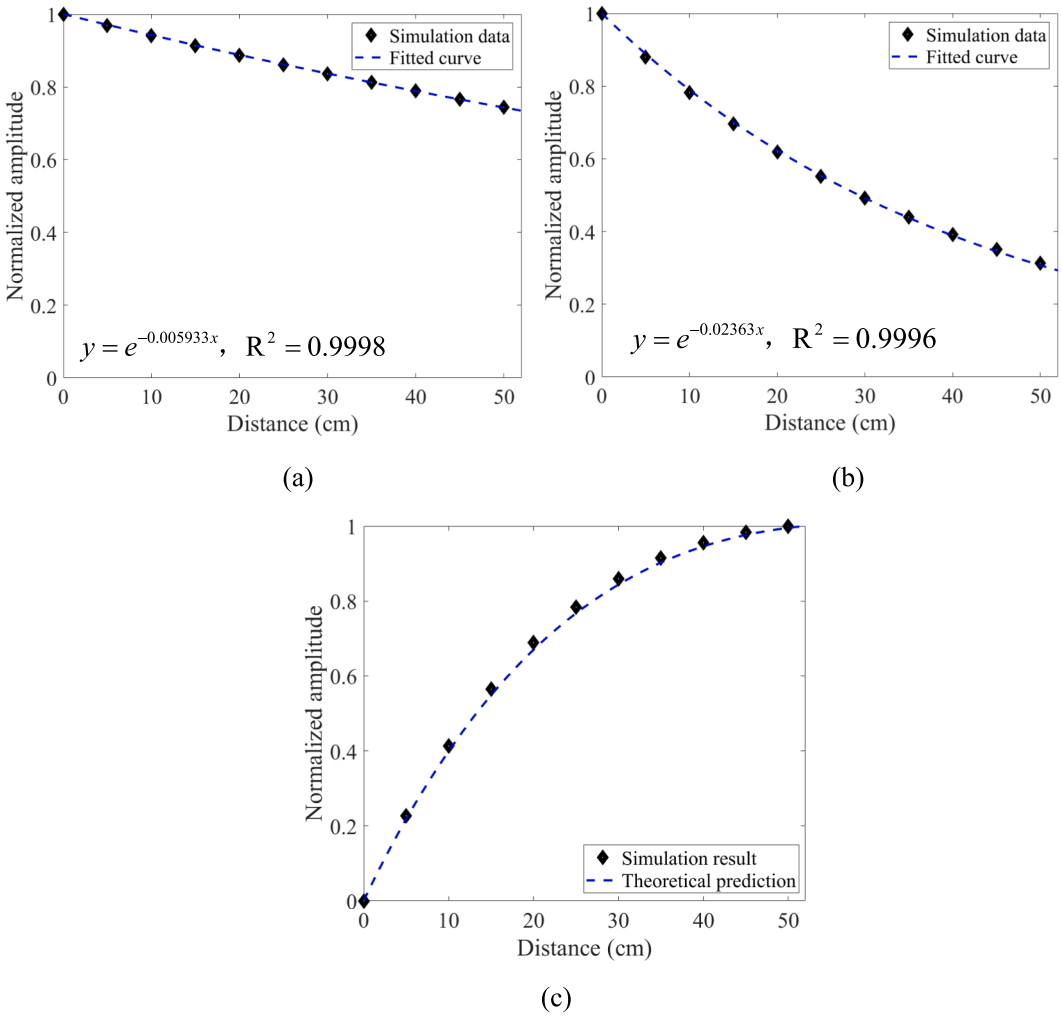

Fig. 6. Influence of low damping ($\widetilde{\lambda} = 1000$ Pa·s, $\widetilde{\mu} = 400$ Pa·s) on the cumulative effect: attenuation patterns of Lamb waves at (a) 100 kHz and (b) 200 kHz; (c) cumulative pattern of the second harmonic Lamb waves.

Reaching a position x, the amplitude of the second harmonic Lamb wave attenuates to $dA_2(f_{2\omega}(x-\xi))$. As a result, the second harmonic Lamb wave amplitude is obtained as

$$A_2(x) = \int_0^x k(A_1 f_\omega(\xi))^2 f_{2\omega}(x-\xi)d\xi \tag{3}$$

Eq. (3) suggests that the cumulative characteristics of the second harmonic Lamb waves in the damped plate can be predicted if the attenuation patterns of the Lamb waves at the fundamental and double frequencies can somehow be obtained. This can be readily done through measuring the Lamb waves at these two frequencies. This way, one can predict the cumulative characteristics of the second harmonic Lamb waves without the specific knowledge on material damping parameters, whose accurate quantification turns out to be difficult in practice. While confirming the variation trend of the second harmonic Lamb waves versus propagation distance, we also intend to use this method to predict the "sweet" zones in the wave propagation path in which the amplitude of the second harmonic Lamb waves is large to facilitate the measurement.

3. Numerical demonstration and validations

Finite element simulations are performed to validate the prediction method described above. Taking the material damping of the plates into account, the cumulative characteristics of the second harmonic Lamb waves are investigated. In addition, the influence of the wave beam divergence is also evaluated.

3.1. Cumulative characteristics of second harmonic Lamb waves in damped plates

First, two-dimensional (2D) simulations are carried out under the plane wave assumption. A finite element model is created in Abaqus as illustrated in Fig. 2. A representative plate with a thickness of 2 mm and a length of 1 m is studied. By combining the Kelvin-Voigt viscoelastic model and the Landau-Lifshitz model [24], we use a constitutive model to characterize the weakly nonlinear material with damping as

$$\sigma = \lambda tr[\varepsilon]I + 2\mu\varepsilon + \widetilde{\lambda} tr[\dot{\varepsilon}]I + 2\widetilde{\mu}\dot{\varepsilon} + \overline{A}\varepsilon^2 + \overline{B}tr[\varepsilon^2]I + 2\overline{B}tr[\varepsilon]\varepsilon + \overline{C}(tr[\varepsilon])^2 I \tag{4}$$

where λ and μ are Lamé constants and $\widetilde{\lambda}$ and $\widetilde{\mu}$ are the two viscosity parameters. $\overline{A}$, $\overline{B}$, and $\overline{C}$ are the Landau third-order elastic constants (TOECs). $\mathbf{I}$ is the identity tensor and the operation tr[] represents the trace. σ and ε are the nominal stress and engineering strain respectively. Note that the second Piola-Kirchhoff stress and the Lagrangian strain are used in the original Landau-Lifshitz model. Since it has been shown that geometric nonlinearities have much less effect than material nonlinearities, the nominal stress and engineering strain can be reasonably

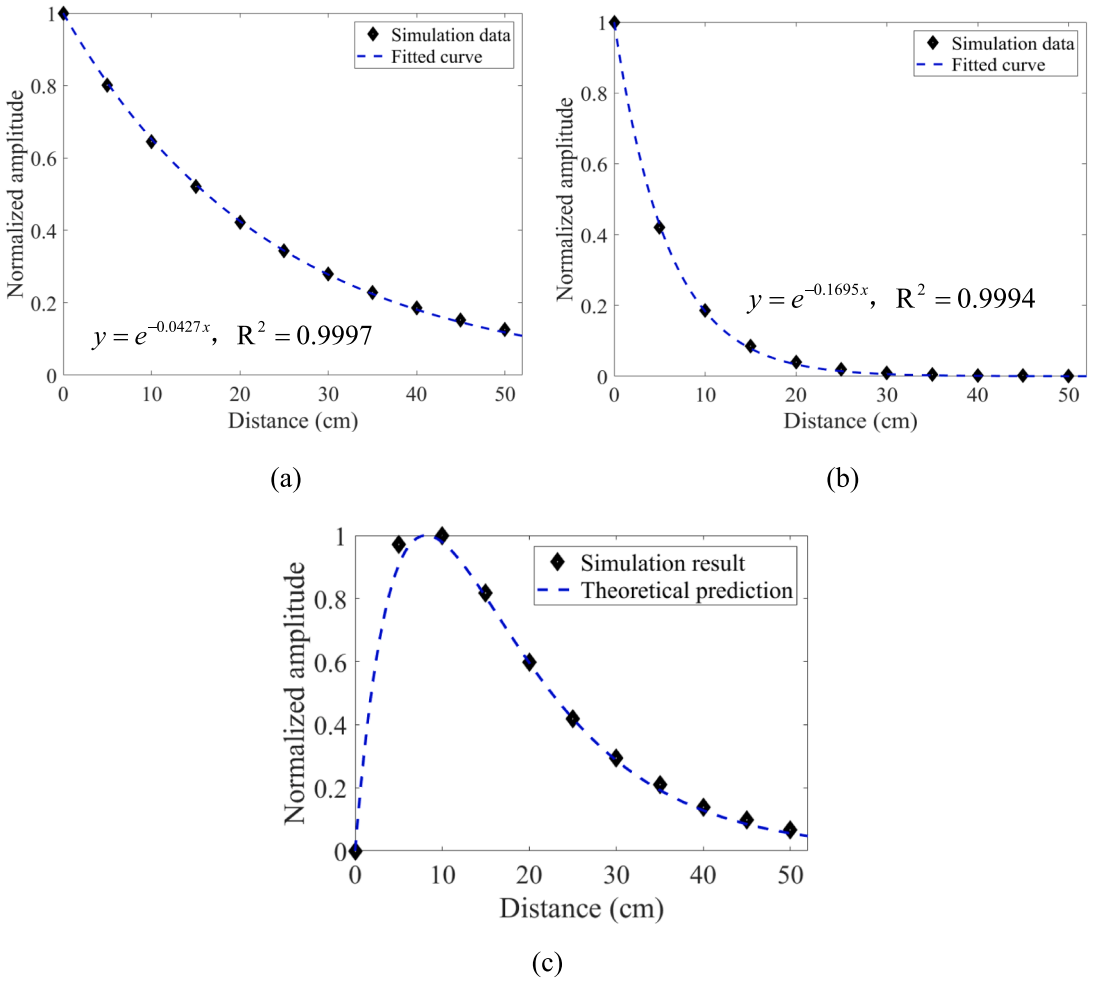

Fig. 7. Influence of high damping ($\tilde{\lambda} = 7500$ Pa·s, $\tilde{\mu} = 3000$ Pa·s) on the cumulative effect: attenuation patterns of Lamb waves at (a) 100 kHz and (b) 200 kHz; (c) cumulative pattern of the second harmonic Lamb waves.

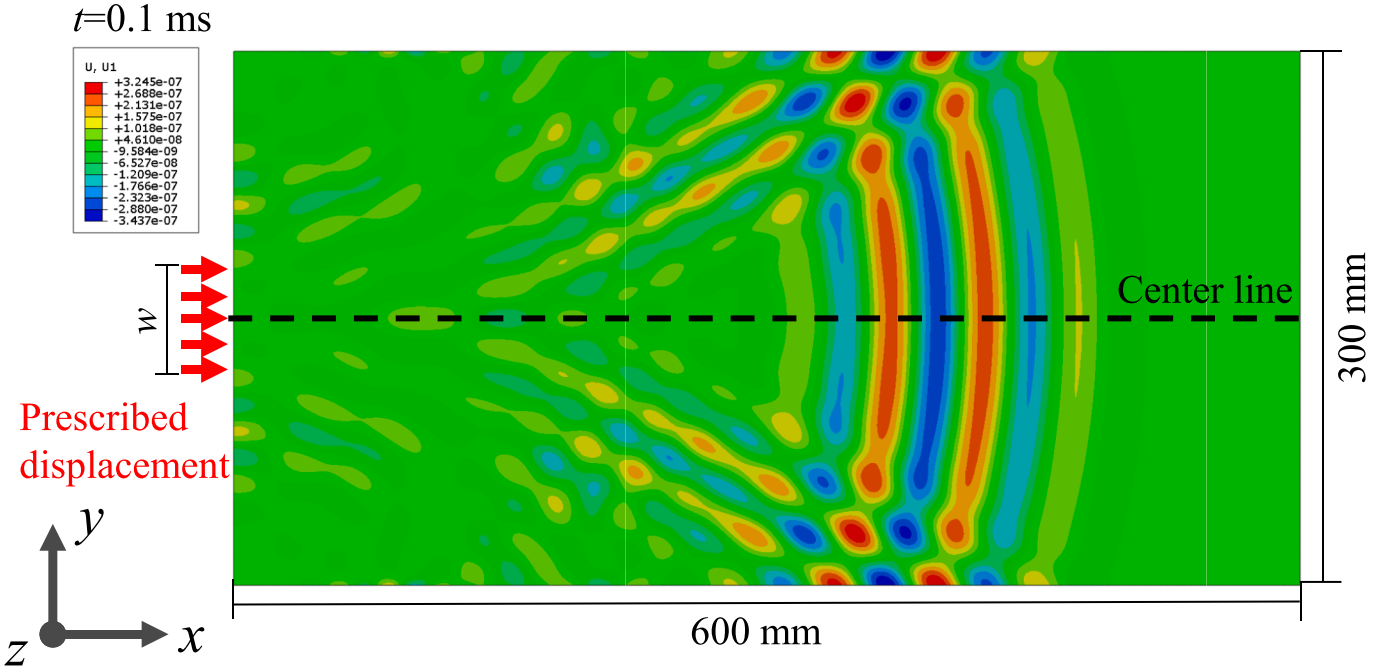

Fig. 8. The 3D finite element model.

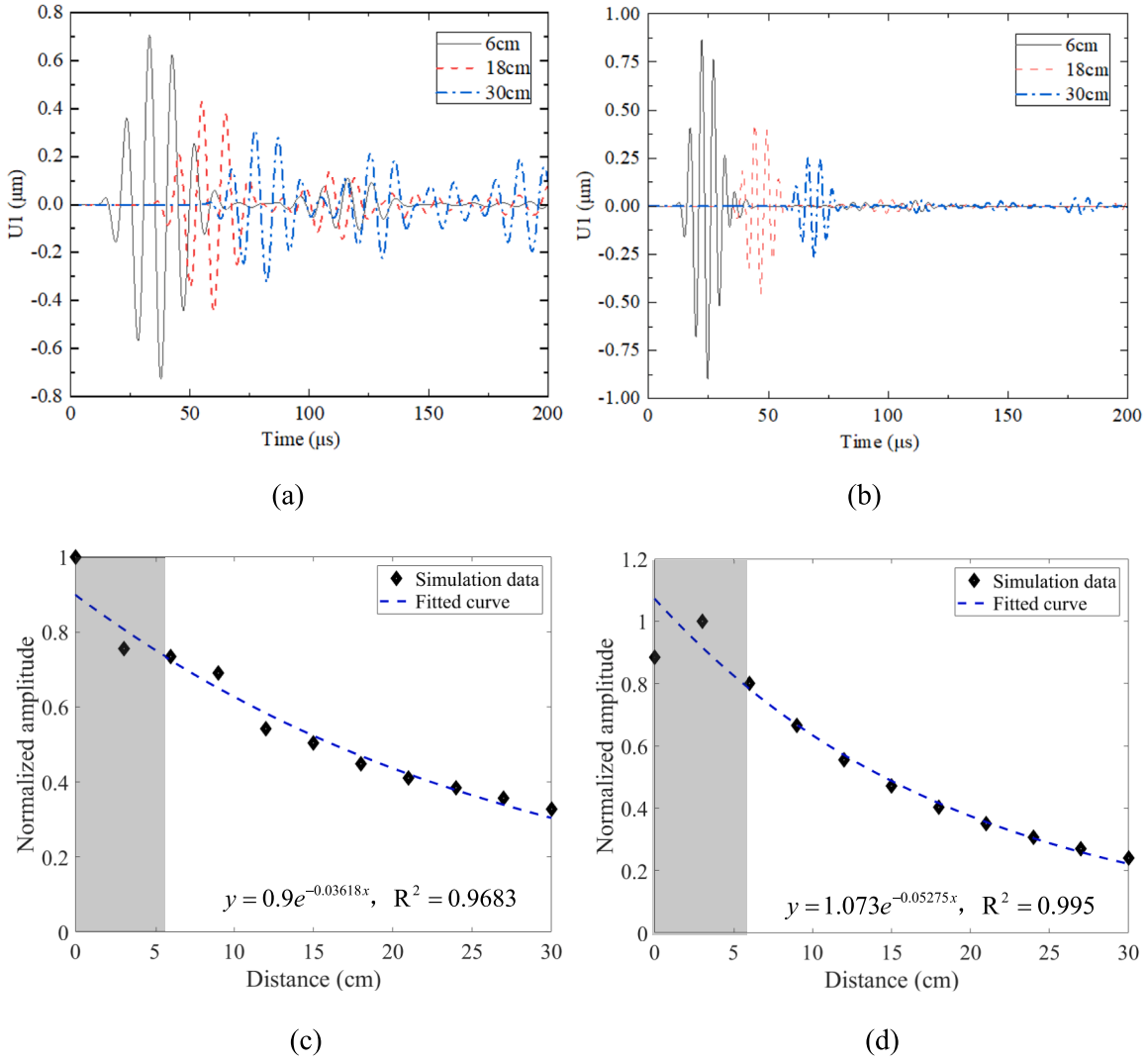

Fig. 9. Typical Lamb wave responses at different positions and their extracted attenuation patterns of: (a) and (c) 100 kHz; (b) and (d) 200 kHz.

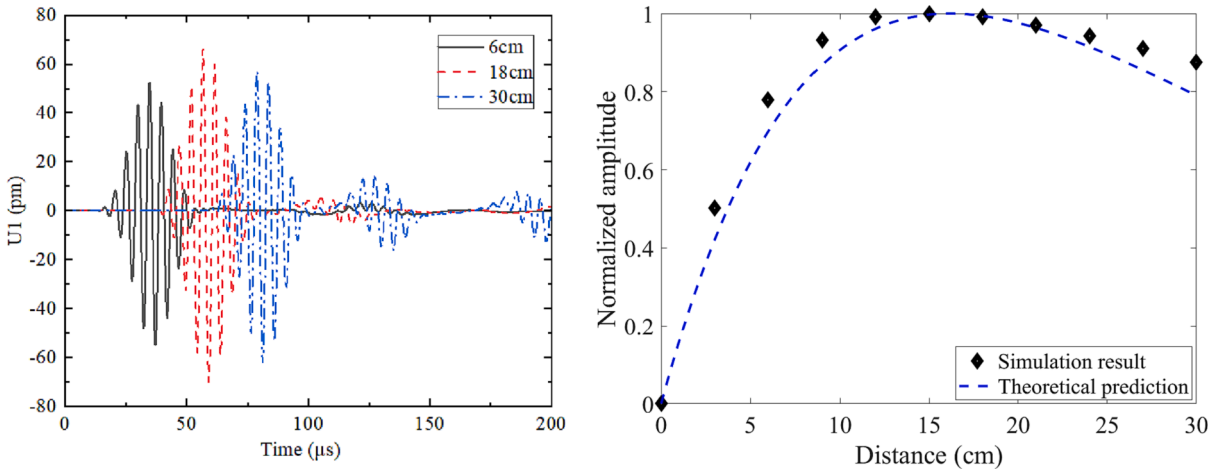

Fig. 10. Cumulative effect of the second harmonic Lamb waves: (a) typical second harmonic responses (b) comparison between the theoretical prediction and numerical data.

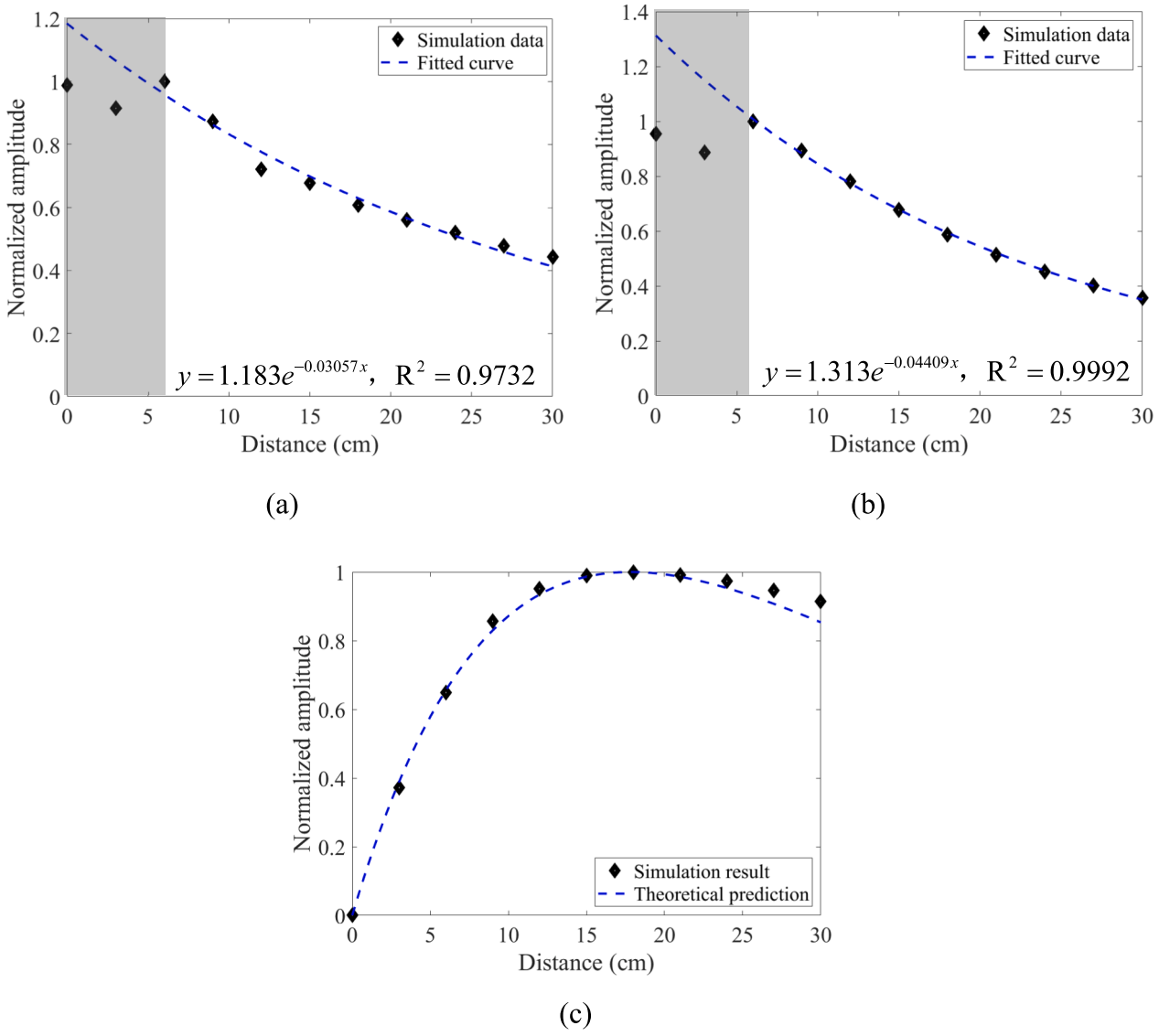

Fig. 11. Influence of weaker wave beam divergence ($w = 7$ cm) on the cumulative effect: attenuation patterns of Lamb waves at (a) 100 kHz and (b) 200 kHz; (c) cumulative pattern of the second harmonic Lamb waves.

used for simplicity. The constitutive model is coded with the user material subroutine (UMAT) in Abaqus. The material parameters used in the simulations are given in Table 1.

A prescribed displacement in the x-direction is uniformly applied to the left end of the plate. Only symmetrical Lamb waves can then be generated. The excitation is a 5-cycle tone burst signal windowed by a Hann function with a center frequency of 100 kHz or 200 kHz. As the frequencies are far below the cut-on frequencies of higher order modes in a 2 mm-thick plate, only the lowest S0 mode waves are generated in the present case. The amplitude is set to 0.1 μm. A fine mesh of 0.5 mm × 0.5 mm is used with more than 40 elements per smallest wavelength. The displacements in the x-direction (U1) of 11 points on the top surface from 0 cm to 50 cm with a step size of 5 cm to the left end are extracted as the output of the system at a sampling frequency of 10 MHz.

Fig. 3(a) and 3(b) show some typical responses at different locations corresponding to the excitations at 100 kHz and 200 kHz, respectively. By tracking the time of flights of the first arrivals, the group velocities are deducted to be 5430 m/s and 5380 m/s for the 100 kHz and 200 kHz waves, respectively, which are very close to the theoretical values of the S0 mode waves. The wave packets after 200 μs in Fig. 3(a) correspond to the reflection of S0 mode waves from the right edge of the plate, which arrive much later than the first arrivals. Therefore, the influence of boundary reflections can be neglected in the subsequent analyses. As there is only a very slight dispersion in the S0 mode waves in the low frequency range, changes in the waveform can hardly be visible during propagation. In addition, the effect of damping is evident from the wave attenuation versus the propagation distance. The material damping leads to a higher attenuation rate for the 200 kHz wave.

The complex Morlet wavelet transform [25] is then applied to extract the Lamb wave amplitudes at different locations. By normalizing the maximum amplitude, the Lamb wave the amplitudes at 100 kHz and 200 kHz corresponding to different propagation distances are obtained in Fig. 4(a) and (b). According to the literature [26,27], the exponential function can be used to extract the attenuation patterns of Lamb waves induced by material damping as

$$f(x) = e^{-bx} \tag{5}$$

In which b is the attenuation factor from which b_1 and b_2 are derived for the waves at fundamental and double frequencies. It can be seen that the exponential function fits the finite element result very well. Substituting the attenuation patterns of Lamb waves into Eq. (3), the amplitude of the second harmonic Lamb waves can be predicted as

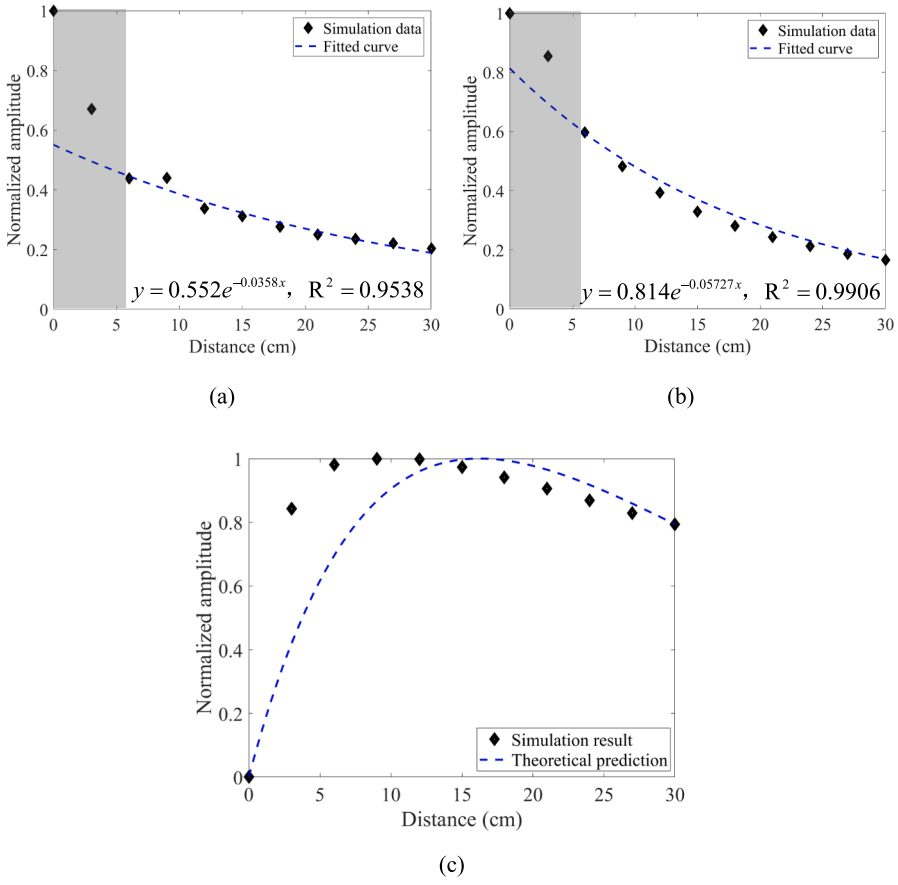

Fig. 12. Influence of stronger wave beam divergence ($w = 3$ cm) on the cumulative effect: attenuation patterns of Lamb waves at (a) 100 kHz and (b) 200 kHz; (c) cumulative pattern of the second harmonic Lamb waves.

$$A_2(x) = \frac{kA_1^2}{b_2 - 2b_1} e^{-b_2 x}\left(e^{(b_2 - 2b_1)x} - 1\right) \tag{6}$$

To verify this, the second harmonic Lamb waves corresponding to the 100 kHz excitation are extracted with the phase inversion method [28,29]. Specifically, a pair of phase-reversed excitations is applied, and the second harmonic components are extracted by averaging the corresponding responses. The second harmonic responses at some representative positions are presented in Fig. 5(a), showing an increasing and then decreasing trend. After extracting their amplitudes using the complex Morlet wavelet transform and normalizing the maximum value, the simulation results are compared with the theoretical prediction in Fig. 5(b). It can be seen that the theoretical result is in good agreement with the numerical data and the "sweet" zone for the maximum amplitude is well predicted by the proposed method.

Two other cases with different damping levels are then considered. The first one is low damping with $\widetilde{\lambda}$ and $\widetilde{\mu}$ set to 1000 and 400 Pa·s respectively. Other parameters are the same as those in Table 1. Following the same procedure, the attenuation patterns of the Lamb waves at 100 kHz and 200 kHz are extracted as shown in Fig. 6(a) and 6 (b). The cumulative effect can then be predicted using Eq. (6) and compared with the finite element result in Fig. 6(c). The second case involves higher damping with $\widetilde{\lambda}$ and $\widetilde{\mu}$ of 7500 and 3000 Pa·s respectively. The attenuation patterns are measured in Fig. 7(a) and 7(b) and the corresponding cumulative feature is presented in Fig. 7(c). In both cases, the theoretical predictions are in good agreement with the finite element results. In addition, we can see that the "sweet" zone of the maximum second harmonic Lamb wave amplitude is shifted forward with increasing damping.

3.2. Influence of wave beam divergence

In practice, Lamb waves are usually generated by transducers of limited size. As a result, the generated Lamb waves are non-planar and attenuate during propagation due to wave beam divergence. To assess the effect of the wave beam divergence, three-dimensional (3D) finite element simulations are carried out, as shown in Fig. 8. The dimensions of the plate are 600 mm × 300 mm × 2 mm. The sizes of the plate are selected to mitigate the influence of boundary reflections from the edges on the S0 mode waves of interest. In the simulations, $\widetilde{\lambda}$ and $\widetilde{\mu}$ are fixed at 1000 and 400 Pa·s respectively, and other parameters can be obtained from Table 1. A prescribed displacement with an amplitude of 1 μm is applied at the left end and uniformly distributed over the entire thickness to excite the Lamb waves in S0 mode. By varying the excitation width w, the level of wave beam divergence can be controlled. The excitation signals are the same as those used in the 2D cases, with excitation frequencies of 100 kHz and 200 kHz. The mesh size is 0.5 mm × 0.5 mm × 0.5 mm. The outputs are the displacements in the x direction (U1) of 11 points on the top surface along the center line from 0 cm to 30 cm, with a step size of 3 cm at the left end. The sampling frequency is set to 20 MHz.

In the first case, the width of the excitation is set to 5 cm. The resulting responses to the 100 kHz and 200 kHz excitations at some typical locations are shown in Fig. 9(a) and 9(b). It is worth noting that the we have tracked the wave propagation process carefully in the simulation to ensure that the boundary reflections do not affect the first arrivals of the signals. The S0 mode wave packets can be clearly seen as the first wave packet in each signal. The complex Morlet wavelet transform is then applied to extract the amplitudes corresponding to different propagation distances as shown in Fig. 9(c) and 9(d). The

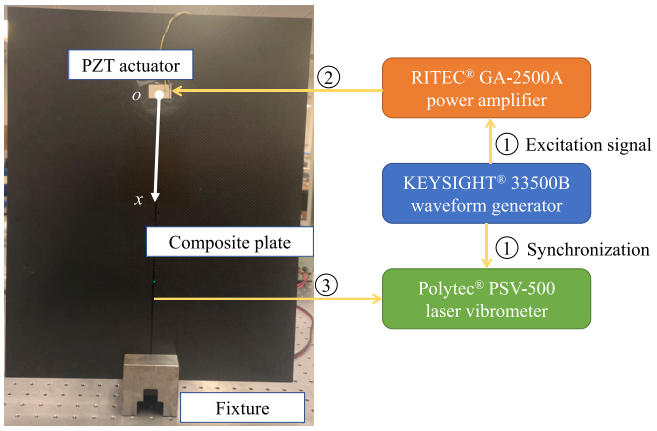

(a)

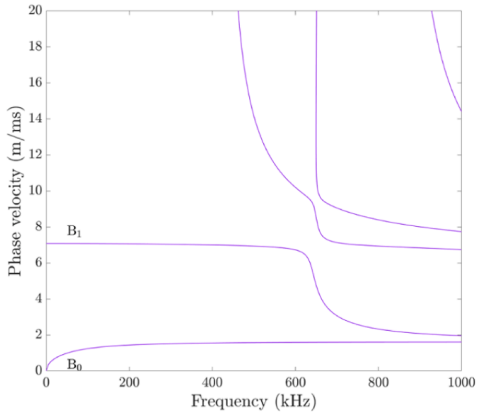

(b)

Fig. 13. (a) Experimental set-up and (b) dispersion curves of Lamb waves propagating at 0° direction in the 12-ply CFRP.

Table 2
Engineering constants of AS4M3502 (single layer).

ρ[kg/m^3]	E_1[GPa]	E_2 [GPa]	G_{12} [GPa]	υ_{12}	υ_{23}
1550	144.6	9.6	6	0.30	0.28

exponential function is used to describe the wave attenuation pattern. In this case, the first two amplitudes corresponding to the 0 and 3 cm propagation distances are not used for curve fitting. This is because the waves at these two positions are more susceptible to near-field effects.

Similarly, the second harmonic Lamb wave responses are then extracted using the phase-inversion method, and typical results are shown in Fig. 10(a). By applying the attenuation patterns of the Lamb waves at the fundamental and double frequencies in Eq. (6), the theoretical predictions of the second harmonic amplitude with respect to the propagation distance are obtained and compared with the numerical results shown in Fig. 10(b). Good agreement is again observed and the "sweet" zone is well predicted.

Considering different levels of wave beam divergence, two additional cases are then considered, In the first case, a 7 cm-wide excitation is used corresponding to a lower wave beam divergence case. Following the same procedure, the attenuation patterns of the waves at 100 kHz and 200 kHz are extracted as shown in Fig. 11(a) and 11(b). The theoretical predictions are shown in Fig. 11(c), which shows a longer cumulative distance. It can be seen that the proposed method also allows an accurate prediction of the cumulative effect. The second case considers a 3 cm-wide excitation with a higher wave beam divergence level, as evidenced by the rapid attenuation of the Lamb waves near the excitation in Fig. 12 (a) and (b). The resulting theoretical prediction is shown in Fig. 12(c), where the cumulative distance becomes shorter. The discrepancy between the theoretical predictions and the numerical results becomes larger because the extracted attenuation patterns cannot accurately characterize the wave attenuation due to the increased wave beam divergence. However, the predicted trend of the second harmonic amplitudes remains consistent with the simulation results. The proposed method can still provide acceptable prediction of the "sweet" zone in practical applications.

To sum up, the proposed method for predicting the cumulative effect of second harmonic Lamb waves is validated by finite element simulations. Both 2D and 3D simulation results confirm the influence of the material damping on the cumulative effect. Specifically, the amplitude of the second harmonic Lamb wave generally undergoes increasing and then decreasing trends, resulting in a "sweet" zone which is conducive to measurement. The results show that the larger the damping and the greater the wave beam divergence, the smaller the cumulative distance becomes. In addition, the linear and nonlinear waves in the 3D simulation results attenuate faster than their counterparts in the 2D scenario for the same level of material damping. The wave beam divergence in the 3D case results in a significant shift of the "sweet" zone towards the excitation source. Meanwhile, it is also found that the proposed method is significantly affected when the wave beam divergence is large, which should be considered in practical applications.

4. Experimental investigations

Finally, experiments are carried out to further validate the proposed prediction method using a 400 mm × 500 mm × 2 mm carbon fiber reinforced plate (CFRP) (shown in Fig. 13(a)). The plate contains 12 layers ($[0°/90°]_6$) made of AS4M3502 (transversely isotropic material). The engineering constants of a single layer are tabulated in Table 2. A 30 mm × 16 mm × 0.5 mm PZT wafer is bonded to the plate for wave excitation. The measurement system works as follows: a KEYSIGHT® 33500B waveform generator is used to generate the excitation signal, which is a tone burst signal windowed by a Hann function. The signal is then amplified by a RITEC® GA-2500A power amplifier and sent to the PZT actuator. The out-of-plane velocity of Lamb waves are measured by a Polytec® PSV-500 vibrometer. Meanwhile, the excitation signal is also sent to the vibrometer to ensure the synchronization of wave generation and reception. The sampling frequency of the vibrometer is set to 5 MHz.

The dispersion curves of the Lamb waves in the composite plate are calculated using Dispersion Calculator in MATLAB. The AS4M3502 with the properties in Table 2 is first selected in the software, followed by the lay-up setup ($[0°/90°]_6$ in this case). Then a wave propagating angle is specified which is 0° to match the experiments. As a result, the dispersion curves of the Lamb waves propagating at 0° direction in the 12-ply CFRP are obtained and shown in Fig. 13(b). Note that the shear horizontal modes are not considered. It can be seen that the B_1 mode Lamb wave is slightly dispersive in the low frequency range, so according to the theory [23], the second harmonic B_1 mode Lamb waves in this frequency range should be cumulative. By sweeping the excitation frequency from 50 kHz to 400 kHz, it is found that the amplitude of the B1 mode wave is maximum at 160 kHz. Therefore, in the following analyses, the excitation signal is determined as a 5-cycle tone burst signal with the center frequency of 160 kHz and its double frequency at 320 kHz.

Following the procedure of the proposed prediction method, the Lamb waves at 160 kHz and 320 kHz are measured along the 0° direction at different locations corresponding to the wave propagation distances ranging from 9 cm to 33 cm in 3 cm increments. Two typical responses corresponding to a distance of 15 cm at 160 kHz and 320 kHz are shown in Fig. 14(a) and (b), respectively. The attenuation of the

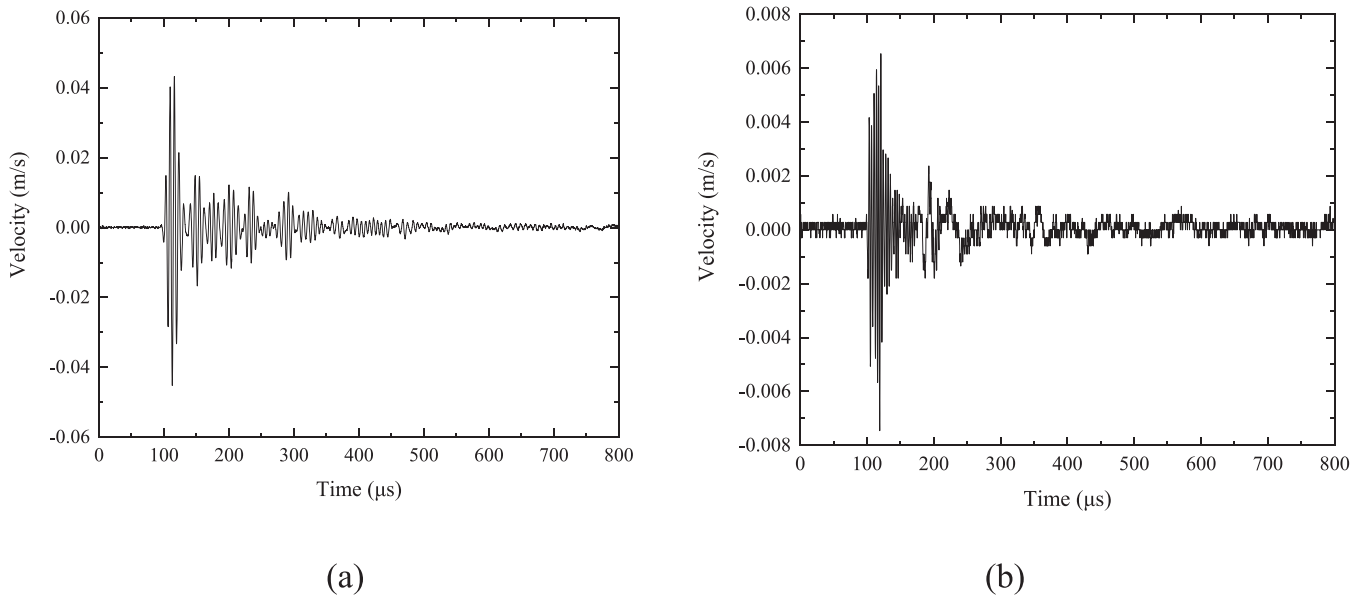

Fig. 14. Typical responses of Lamb waves at $x = 15$ cm of (a) 160 kHz and (b) 320 kHz.

Lamb waves in this structure is evident due to both material damping and wave beam divergence.

The first wave packets corresponding to different wave propagation distances are then examined with typical results shown in Fig. 15(a) and (b). By tracking the first peaks in the signals (marked by triangles), the phase velocities of the Lamb waves at 160 kHz and 320 kHz are calculated to be 6977 m/s and 7058 m/s respectively, which are very close to the theoretical values (7065 m/s at 160 kHz and 7029 m/s at 320 kHz). It is therefore concluded that the first wave packets are indeed B1 mode Lamb waves. The amplitudes of the first peaks for Lamb waves at different locations are then extracted as shown in Fig. 15 (c) and (d). The reason for choosing the first peak is to minimize the influence of reflections as explained in the literature [30]. Curve fitting is then performed to determine the attenuation pattern of the B_1 mode Lamb waves at 160 kHz and 320 kHz. As mentioned above, the responses corresponding to short propagation distances are more susceptible to near-field effects, so the first two data are excluded in the curve fitting process. Based on the extracted wave attenuation pattern, the amplitude of the second harmonic Lamb waves can be predicted according to Eq. (6).

The second harmonic responses corresponding to the 160 kHz excitation are then extracted using the phase-inversion method. A Butterworth filter with passbands from 240 kHz to 400 kHz [28] is then applied to purify the second harmonic responses at different locations, and typical results are shown in Fig. 16 (a). It can be seen that the second harmonic Lamb waves first increase and then decrease with the propagation distance. To quantify the variation pattern, the complex Morlet wavelet transform is used in Fig. 16 (b) to extract the wave amplitudes at 320 kHz. Through normalization to the maximum value, the cumulative characteristics of the second harmonic Lamb waves are obtained and compared with the theoretical prediction in Fig. 16(c). The measurements are repeated four times and the error bars are calculated to demonstrate the reliability of the results. It can be seen that discrepancy increases the further the propagation distance. This can be attributed to the inevitable nonlinearities in the measurement system, such as the instrumentation nonlinearity and nonlinearities at the actuation section [28,29,31]. The second harmonic Lamb waves generated by these nonlinear sources are not cumulative therefore decay monotonically during propagation. Therefore, the further the propagation distance, the more the amplitude of the second harmonic Lamb wave is affected. Nonetheless, the theoretical predictions are still in agreement with the experimental results in terms of the variation trend and the "sweet" zone, which can still provide guidance for NDE and SHM applications.

As a final remark, this work aims to propose a method to characterize the cumulative effect of the second harmonic Lamb waves in a lossy plate. We intended to demonstrate the dominant physical phenomena concerning wave propagation using simple models and verify their extensibility to more general cases. More specifically, we would reiterate that the proposed method is simple and general regardless of the anisotropy of the plate. Therefore, we used an isotropic material in the simulations for convenience and an anisotropic CFRP in the experiments to validate the proposed method from different perspectives. In fact, a practical consideration is that it is very difficult to build an accurate constitutive model for nonlinear anisotropic material with damping. Even if we opted an existing one, it would have been extremely difficult to accurately identify all the parameters involved. Therefore, we decided to use an isotropic plate in the simulations by following the common practice reported in literature [24]. On the other hand, the CFRP is a typical lossy structure which has been widely used for various engineering applications. We believe using a CFRP in the experiments to confirm the numerically predicted physical phenomena in simpler structures would be more meaningful and conclusive in showing the generic characters of the wave propagation in a lossy medium, in addition to the practical relevance of the CFRP for engineering applications. In return, such a strategy (using different materials in the simulations and experiments) allows to demonstrate the versatility and flexibility of the proposed method.

5. Conclusions

In this paper, the cumulative effect of second harmonic Lamb waves in lossy plates with damping is investigated. A method is proposed to predict the cumulative properties and the location of the maximum second harmonic Lamb wave amplitude ("sweet" zone). Finite element investigations are first carried out to validate the proposed method. In addition, the influence of the wave beam divergence is also evaluated to better understand the cumulative effects. Finally, experiments are performed on a composite plate to further validate the method.

Due to material damping, the cumulative second harmonic Lamb waves generally exhibit an increasing and then decreasing trend. By capturing the attenuation patterns of Lamb waves at fundamental and double frequencies, the proposed method can predict the cumulative features, as demonstrated by both numerical and experimental results. It

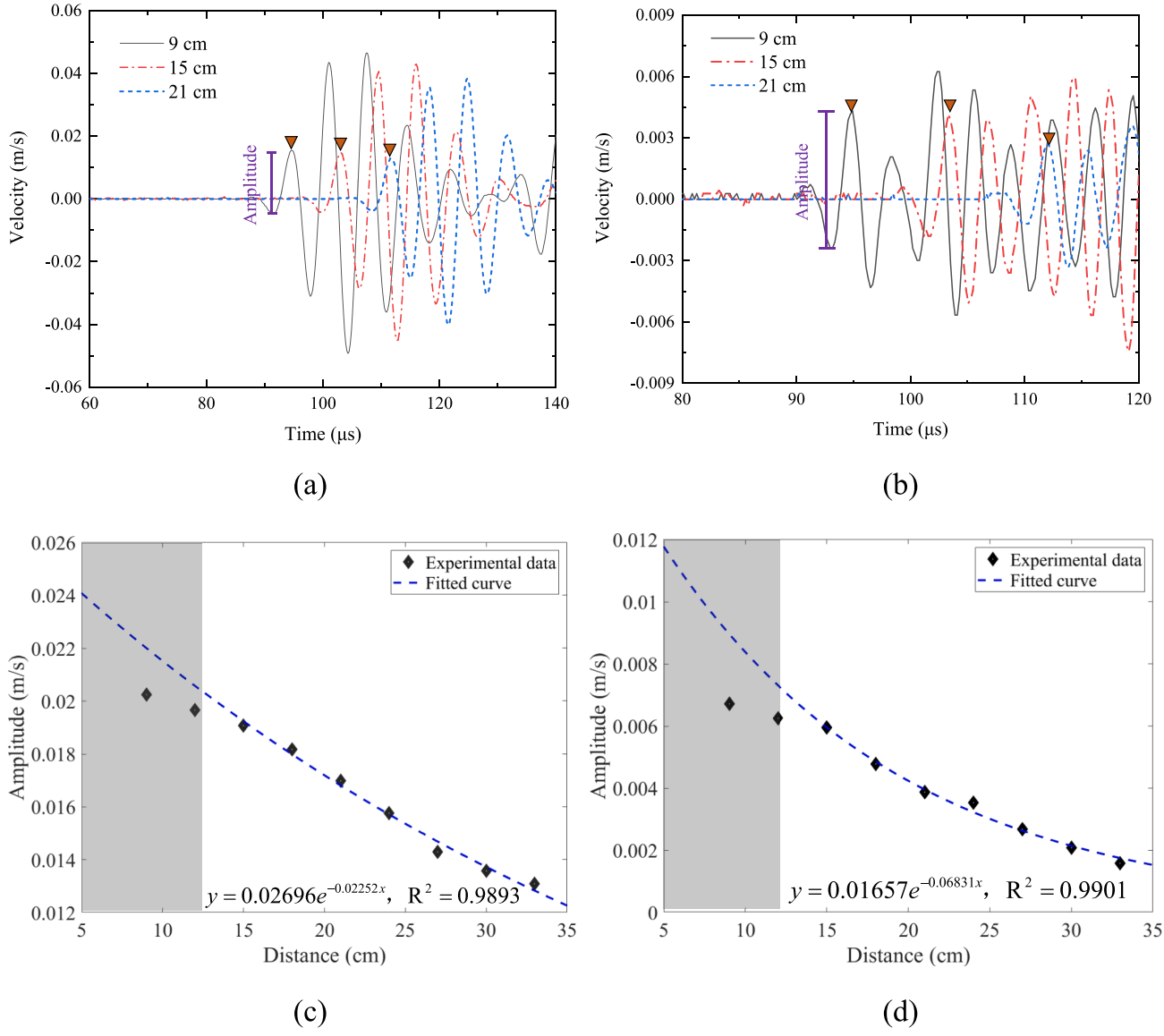

Fig. 15. Typical Lamb wave responses at different positions and their extracted attenuation patterns of: (a) and (c) 160 kHz; (b) and (d) 320 kHz.

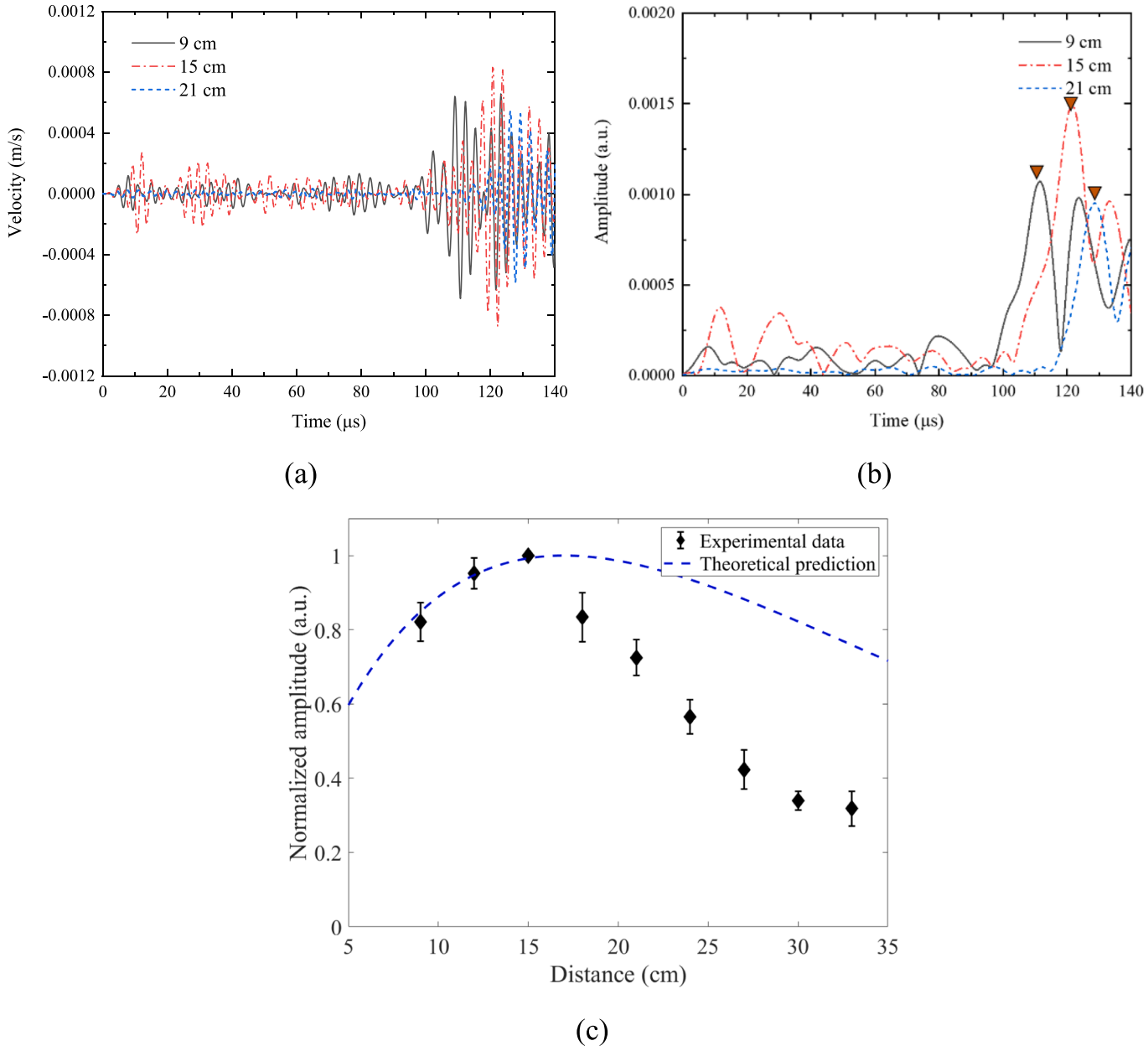

Fig. 16. Cumulative effect of the second harmonic Lamb waves: (a) typical time-domain responses; (b) corresponding wavelet coefficients; (c)comparison between the theoretical prediction and experimental results.

is found that larger the damping and the greater the wave beam divergence, the smaller the cumulative distance. In addition, strong wave beam divergence can significantly affect the prediction accuracy.

The understanding of the cumulative characteristics of the second harmonic Lamb waves and the availability of the proposed method can guide further NDE and SHM applications in two ways. First, a "sweet" zone with relatively large amplitude of the second harmonic Lamb waves can be identified in advance to facilitate the measurement. Second, one needs to be alert to the detrimental effects of wave beam divergence in practical applications for better system design.

CRediT authorship contribution statement

Shengbo Shan: Conceptualization, Funding acquisition, Investigation, Methodology, Supervision, Validation, Writing – original draft. **Yuanman Zhang:** Data curation, Investigation, Validation, Writing – review & editing. **Liaoliao Cheng:** Data curation, Validation, Writing – review & editing. **Yang Song:** Investigation, Validation. **Yongdong Pan:** Data curation, Resources, Supervision. **Li Cheng:** Funding acquisition, Supervision, Validation, Writing – review & editing.

Declaration of competing interest

The authors declare that they have no known competing financial interests or personal relationships that could have appeared to influence the work reported in this paper.

Data availability

Data will be made available on request.

Acknowledgments

The work was supported by grants from the National Natural Science Foundations of China (12302114), the Research Grants Council of Hong Kong Special Administrative Region (PolyU 152013/21E), the Natural Science Foundation of Shanghai (22ZR1462700), the Fundamental Research Funds for the Central Universities and the Innovation and Technology Commission of the HKSAR Government to the Hong Kong Branch of National Rail Transit Electrification and Automation Engineering Technology Research Center.

References

[1] K.H. Matlack, J.-Y. Kim, L.J. Jacobs, J. Qu, Review of second harmonic generation measurement techniques for material state determination in metals, J. Nondestr. Eval. 34 (2015) 273.
[2] K.-Y. Jhang, Nonlinear ultrasonic techniques for nondestructive assessment of micro damage in material: a review, Int. J. Precis. Eng. Manuf. 10 (2009) 123–135.
[3] H. Yun, R. Rayhana, S. Pant, M. Genest, Z. Liu, Nonlinear ultrasonic testing and data analytics for damage characterization: a review, Measurement 186 (2021), 110155.
[4] V.K. Chillara, C.J. Lissenden, Review of nonlinear ultrasonic guided wave nondestructive evaluation: theory, numerics, and experiments, Opt. Eng. 55 (2016) 011002.
[5] Y. Liu, V.K. Chillara, C.J. Lissenden, J.L. Rose, Third harmonic shear horizontal and Rayleigh Lamb waves in weakly nonlinear plates, J. Appl. Phys. 114 (2013), 114908.
[6] M. Hasanian, C.J. Lissenden, Second order harmonic guided wave mutual interactions in plate: vector analysis, numerical simulation, and experimental results, J. Appl. Phys. 122 (2017), 084901.
[7] G. Zhao, M. Jiang, Y. Luo, Q. Sui, Third harmonic approximate phase velocity matching nonlinear early fatigue damage detection, Measurement 189 (2022), 110518.
[8] C.J. Lissenden, Nonlinear ultrasonic guided waves—principles for nondestructive evaluation, J. Appl. Phys. 129 (2021), 021101.
[9] S. Sampath, H. Sohn, Cubic nonlinearity parameter measurement and material degradation detection using nonlinear ultrasonic three-wave mixing, Ultrasonics 121 (2022), 106670.
[10] X. Ding, Y. Zhao, M. Deng, G. Shui, N. Hu, One-way Lamb mixing method in thin plates with randomly distributed micro-cracks, Int. J. Mech. Sci. 171 (2020), 105371.
[11] H. Chen, G. Zhang, D. Fan, L. Fang, L. Huang, Nonlinear lamb wave analysis for microdefect identification in mechanical structural health assessment, Measurement 164 (2020), 108026.
[12] V. Marcantonio, D. Monarca, A. Colantoni, M. Cecchini, Ultrasonic waves for materials evaluation in fatigue, thermal and corrosion damage: a review, Mech. Syst. Sig. Process. 120 (2019) 32–42.
[13] W. Li, J. Xiao, M. Deng, Micro-defect imaging with an improved resolution using nonlinear ultrasonic Lamb waves, J. Appl. Phys. 131 (2022), 185101.
[14] H. Chen, M. Deng, G. Gao, C. Xu, N. Hu, et al., Characterization of interfacial property of a two-layered plate using a nonlinear low-frequency Lamb wave approach, Ultrasonics 124 (2022), 106741.
[15] F. Masurkar, W.T. Peter, N.P. Yelve, Theoretical and experimental measurement of intrinsic and fatigue induced material nonlinearities using Lamb wave based nonlinearity parameters, Measurement 151 (2020), 107148.
[16] W. De Lima, M. Hamilton, Finite-amplitude waves in isotropic elastic plates, J. Sound Vibr. 265 (2003) 819–839.
[17] M.F. Müller, J.-Y. Kim, J. Qu, L.J. Jacobs, Characteristics of second harmonic generation of Lamb waves in nonlinear elastic plates, J. Acoust. Soc. Am. 127 (2010) 2141–2152.
[18] M. Deng, Analysis of second-harmonic generation of Lamb modes using a modal analysis approach, J. Appl. Phys. 94 (2003) 4152–4159.
[19] W. Li, B. Chen, Y. Cho, Nonlinear feature of phase matched Lamb waves in solid plate, Appl. Acoust. 160 (2020), 107124.
[20] Y. Liu, V.K. Chillara, C.J. Lissenden, On selection of primary modes for generation of strong internally resonant second harmonics in plate, J. Sound Vib. 332 (2013) 4517–4528.
[21] X. Wan, P. Tse, G. Xu, T. Tao, Q. Zhang, Analytical and numerical studies of approximate phase velocity matching based nonlinear S0 mode Lamb waves for the detection of evenly distributed microstructural changes, Smart Mater. Struct. 25 (2016), 045023.
[22] P. Zuo, Y. Zhou, Z. Fan, Numerical and experimental investigation of nonlinear ultrasonic Lamb waves at low frequency, Appl. Phys. Lett. 109 (2016), 021902.
[23] J. Zhao, V.K. Chillara, B. Ren, H. Cho, J. Qiu, et al., Second harmonic generation in composites: Theoretical and numerical analyses, J. Appl. Phys. 119 (2016), 064902.
[24] K. Kanda, T. Sugiura, Internally resonant guided waves arising from quadratic classical nonlinearities with damping, Int. J. Solids Struct. 216 (2021) 250–257.
[25] S. Shan, J. Qiu, C. Zhang, H. Ji, L. Cheng, Multi-damage localization on large complex structures through an extended delay-and-sum based method, Struct. Health Monit. 15 (2016) 50–64.
[26] H. Mei, V. Giurgiutiu, Guided wave excitation and propagation in damped composite plates, Struct. Health Monit. 18 (2019) 690–714.
[27] M. Gresil, V. Giurgiutiu, Prediction of attenuated guided waves propagation in carbon fiber composites using Rayleigh damping model, J. Intell. Mater. Syst. Struct. 26 (2015) 2151–2169.
[28] Z. Liu, S. Shan, L. Cheng, Nonlinear-Lamb-wave-based plastic damage detection assisted by topologically designed metamaterial filters, Struct. Health Monit. 22 (2023) 1828–1843.
[29] S. Shan, L. Cheng, P. Li, Adhesive nonlinearity in Lamb-wave-based structural health monitoring systems, Smart Mater. Struct. 26 (2016), 025019.
[30] S. Shan, L. Cheng, F. Wen, Characterization of nonplanar second harmonic Lamb waves with a refined nonlinear parameter, J. Nondestruct. Eval. Diagnost. Prognost. Eng. Syst. 1 (2018).
[31] S. Shan, F. Wen, L. Cheng, Purified nonlinear guided waves through a metamaterial filter for inspection of material microstructural changes, Smart Mater. Struct. 30 (2021), 095017.